International Journal of Heat and Mass Transfer 53 (2010) 4047–4059

Contents lists available at ScienceDirect

International Journal of Heat and Mass Transfer

journal homepage: www.elsevier.com/locate/ijhmt

The peridynamic formulation for transient heat conduction

Florin Bobaru *, Monchai Duangpanya

Department of Engineering Mechanics, University of Nebraska-Lincoln, Lincoln, NE 68588-0526, USA

ARTICLE INFO

Article history:
Received 17 November 2009
Received in revised form 16 April 2010
Accepted 16 April 2010

Keywords:
Peridynamics
Nonlocal methods
Transient heat and mass transfer
Heat conduction
Damage

ABSTRACT

In bodies where discontinuities, like cracks, emerge and interact, the classical equations for heat and mass transfer are not well suited. We propose a peridynamic model for transient heat (or mass) transfer which is valid when the body undergoes damage or evolving cracks. We use a constructive approach to find the peridynamic formulation for heat transfer and test the numerical convergence to the classical solutions in the limit of the horizon (the nonlocal parameter) going to zero for several one-dimensional problems with different types of boundary conditions. We observe an interesting property of the peridynamic solution: when two *m*-convergence curves, corresponding to two different horizons, for the solution at a point and an instant intersect, the intersection point is also the exact classical (local) solution. The present formulation can be easily extended to higher dimensions and be coupled with the mechanical peridynamic description for thermomechanical analyses of fracturing bodies, or for heat and mass transfer in bodies with evolving material discontinuities.

1. Introduction and literature review

Nonlocal heat and mass transfer models have been proposed in the past in order to better represent, for example, heat conduction at low temperatures, heat conduction in short-pulse-laser heating, and more generally in steep temperature gradients [1–4]. Motivated by the effects of the material microstructure on the thermal response, a different avenue that uses ensemble averaging techniques has been used in [5,6] to arrive at nonlocal models for heat conduction. The averaging of gradients over certain regions has previously been used in nonlocal models for elasticity and thermo-elasticity in [7,8] (for the elastic response) and [9,10] (for the thermo-elastic response). An axiomatic treatment of irreversible thermodynamics of nonlocal systems is given in [11]. Many of the nonlocal theories for heat-conduction lead to hyperbolic equations and thus to a finite speed of propagation of heat. A thermodynamically consistent description of heat conduction with finite speed of heat propagation is given in [12].

An area where the existing local or nonlocal models cannot be directly applied is the set of problems in which discontinuities in the analyzed body emerge, interact, and evolve. This is the case of, for example, dynamic fracture and fragmentation of materials, granular materials flow etc. One of the great challenges in dynamic fracture listed in [13] is about the physics of dynamic fracture in the presence of thermal gradients. Recent experiments in dynamic fracture of brittle polymeric materials have shown [14] that the crack-tip temperature may even drop significantly upon rapid loading. Temperature-dependent transition from trans-granular to inter-granular fracture can take place under thermomechanical loading as recently reported in [15]. These thermomechanical effects may also be important in the ductile to brittle transition and deserves inclusion in modeling the crack-tip thermodynamics [13]. The need for special computational techniques in using the aforementioned methods in such problems has to do with the fact that spatial gradients (first or second order gradients) appear in these formulations. Such gradients loose meaning (or require redefining the body which leads to complicated implementation methods) once strong discontinuities, such as cracks, or other types of discontinuities emerge in a body. The examples of fragmenting solids under high-velocity impact, thermal fatigue cracking in composites, dynamics of granular materials, or breaking of a fluid jet are some cases, relevant in many disciplines, where situations of spontaneous material discontinuities are generated.

The nonlocal continuum concept has emerged as an effective means for regularizing the boundary value problems with strain softening, capturing the size effects and avoiding spurious localization that gives rise to pathological mesh sensitivity in numerical computations. A great variety of nonlocal models for modeling damage and plastic flow have appeared during the last two decades (see [16]). Conventional continuum mechanics models of inelastic deformation processes are size scale independent. There is considerable experimental evidence that plastic flow in crystalline solids is inherently size dependent over a size scale that ranges from a fraction of a micrometer to 100 mm or so. It is over this mesoscale size range that key deformation and fracture processes

* Corresponding author. Tel.: +1 402 472 8348.
E-mail address: fbobaru2@unl.edu (F. Bobaru).

0017-9310/$ - see front matter © 2010 Elsevier Ltd. All rights reserved.
doi:10.1016/j.ijheatmasstransfer.2010.05.024

Nomenclature

c	specific heat capacity (J/kg K)	m	ratio of horizon and the length (volume) of node (x)
d	distance (m)	Q	peridynamic heat-flux (W/m^2)
$\boldsymbol{e}$	unit director vector	t	time (s)
e_0	critical relative elongation of a peridynamic bond	w	heat source (W/m^3)
f	heat-flux (W/m^2)	α	thermal diffusivity (m^2/s)
H_x	horizon of point x (m)	δ	peridynamic horizon (m)
K	conductivity of a t-bond (W/mK (in 1D))	κ	thermal conductivity (W/mK)
k	micro-conductivity of a t-bond (W/m^{2}K (in 1D))	ρ	density (kg/m^3)
L	length of bar (m)	θ	temperature (°C)

in a variety of structural and electronic materials take place. Gradient-based nonlocal models in plasticity have appeared in, for example, [17–21]. The physical reasons that impose the use of nonlocal models include [16]: (1) heterogeneity of microstructure and its homogenization on a small scale on which the smoothed strain field cannot be considered as uniform (for instance, in concrete, the maximum aggregate size and spacing are important parameters that influence the size of the nonlocal effects); (2) distributed cracking and damage is physically observed yet impossible to simulate numerically with local continuum models; (3) the growth of a microcrack is not decided by the local stress or strain tensor at the continuum point corresponding to the microcrack center but by the overall energy release from a finite volume surrounding the whole microcrack.

The nonlocal model introduced in this paper for heat transfer is motivated by the need of a *simple* mathematical theory and computational model that is mathematically consistent and can work when, in the conducting body, cracks or other types of discontinuities, form, interact, and evolve in general. The model is also useful for modeling heat transfer in materials that are highly thermally heterogeneous. For this purpose we will use the ideas in the peridynamic reformulation of classical mechanics, developed originally in [22]. The term peridynamics comes from the Greek roots for "near" and "force". An important generalization of the theory has appeared in [23]. The nonlocal model presented here for heat transfer differs from previous nonlocal models in that there are no gradients (or volume-averages of such gradients) of the temperature field in the formulation. Spatial integration, rather than differentiation, is used and this leads to a mathematically consistent formulation, even when strong discontinuities appear in the temperature field due to breaking and fragmentation of the material. While we mainly focus on heat-transfer problems, everything in this paper can be directly extended to mass transfer problems by using the well known analogies between these two phenomena (see, e.g., [24]).

The peridynamic theory has been successfully applied to model brittle fracture [25–28], rupture of membranes and nanofiber networks [29,30], spallation [31], damage in composite materials [32], trans-granular and inter-granular crack propagation in polycrystalline ceramics [33], phase transformations [34], plastic and visco-plastic deformation [35,36].

This is the first *constructive approach* to obtain the peridynamic equations from physical principles. In previous peridynamic models (for elasticity etc.) the peridynamic equations were postulated. Here we arrive at the peridynamic formulation (for heat transfer in a bar) following a procedure similar to the one used in [37], in which the classical, local, heat-transfer equations are derived. At a certain step in the derivation, we depart from the path taken in [37] and avoid taking the limit that leads to the classical PDE for heat conduction. We remark that the approach proposed here eliminates the need of showing, theoretically, that the peridynamic formulation converges, in the limit of its nonlocal parameter going to zero, to the classical formulation, as it is done for elasticity in, for example, [38]. We perform numerical tests that show numerical linear and super-linear convergence rates of the peridynamic solution to the classical solutions in the limit of the horizon going to zero (using the notion of δ-convergence [39]). We also observe an interesting property of the peridynamic solutions: when two m-convergence curves corresponding to two different horizon sizes for the solution at a point and at a certain time intersect, the intersection point is also the value of the exact classical solution. This issue needs will be further investigated in the future since it may provide a way to recover the classical exact solution at a point not only by taking the limit of the peridynamic horizon to zero, but also by finding the intersection point, if it exists, of two m-convergence curves for any two horizons.

2. Peridynamic formulation for heat conduction

We first briefly recall the derivation of the classical heat-transfer equation from [37]. Assume an infinite plate, of thickness d bounded by two parallel planes, P and $\widehat{P}$. The two planes are kept at different temperatures, θ and $\hat{\theta}$, with $\hat{\theta} > \theta$. Consider a cylinder as in Fig. 1, with the area of the surfaces S and $\widehat{S}$ being equal to s. We also assume that there is no heat transfer through the cylinder's side surface A. The quantity of heat which flows between the two planes over the area s in t seconds is equal to:

$$\frac{\kappa(\hat{\theta}-\theta)st}{d}. \tag{1}$$

Here κ is the material's thermal conductivity. On the other hand, let f and $\hat{f}$ be the heat-flux per unit time and unit area across the surfaces S and $\widehat{S}$, through $\boldsymbol{x}$ and $\hat{\boldsymbol{x}}$, respectively. Assuming that the flow across the side surface A (see Fig. 1) of the cylinder is negligible, then the rate of heat flow into the cylinder is

$$s(\hat{f}-f). \tag{2}$$

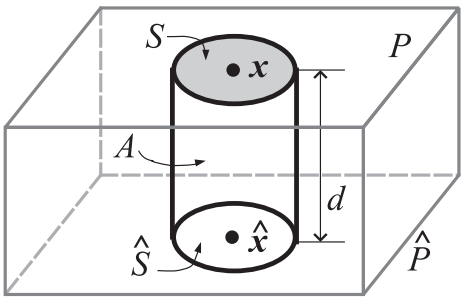

Fig. 1. The heat transfer in a plate bounded by two planes at different temperatures.

If we now define θ_a as the average temperature in the cylinder, then the rate at which the cylinder gains heat is

$$\rho c s d \frac{\partial \theta_a}{\partial t}. \tag{3}$$

Thus, the expressions in Eqs. (1)–(3), per unit area and per unit time, give:

$$\rho c d \frac{\partial \theta_a}{\partial t} \approx \hat{f} - f = \frac{\kappa(\hat{\theta} - \theta)}{d}. \tag{4}$$

This is where we depart from the classical approach, which assumes the distance d between $\boldsymbol{x}$ and $\hat{\boldsymbol{x}}$ (the thickness of the plate) goes to zero and the relationship above becomes an equation written in terms of the spatial gradient of the temperature field (see [37]). Here and below, for simplicity, we consider the density and the heat capacity to be constant. The case of variable density and heat capacity is an immediate extension of the formulation presented here.

For our peridynamic formulation of the heat diffusion equation we consider a body occupying a region Ω in the three-dimensional space (see Fig. 2). The body is composed of material points that have associated mass and volume. We consider that each such material point is connected to the rest of the points in the body Ω via "*thermal conductors*", or "*thermal bonds*". In short, we will call these connections "*t-bonds*". The derivation below is for the case of one-dimensional transient heat transfer in a bar, see Figs. 2 and 3. The extension to two and three-dimensional heat transfer is immediate and will be reported in a future publication.

Let $\boldsymbol{e}$ be a unit vector along the bar. The heat is transferred between point $\boldsymbol{x}$ and any point $\hat{\boldsymbol{x}}$, along the direction of the t-bond vector $\hat{\boldsymbol{x}} - \boldsymbol{x}$, which is collinear with the director vector $\boldsymbol{e}$. It is reasonable to assume that the interaction distance for every material point is limited to a certain region, called *horizon* $\mathcal{H}$, which we take, for convenience, to be spherical of radius δ (see Figs. 2 and 3).

For each of the t-bonds in Fig. 3 we repeat the reasoning above with the same assumption used before: the t-bonds are "insulated" so that there is no heat transfer along the t-bonds between them. We aim to find the peridynamic equation of heat transfer for the point $\boldsymbol{x} \in \Omega$. Writing Eq. (4) as an equation even without taking the limit, gives:

$$\rho c(\hat{\boldsymbol{x}} - \boldsymbol{x}) \cdot \boldsymbol{e} \frac{\partial \theta_a(\boldsymbol{x}, \hat{\boldsymbol{x}}, t)}{\partial t} = K(\boldsymbol{x}, \hat{\boldsymbol{x}}) \frac{\theta(\hat{\boldsymbol{x}}, t) - \theta(\boldsymbol{x}, t)}{(\hat{\boldsymbol{x}} - \boldsymbol{x}) \cdot \boldsymbol{e}}, \tag{5}$$

where $\theta_a(\boldsymbol{x}, \hat{\boldsymbol{x}}, t)$ is the average temperature along the t-bond $(\boldsymbol{x}, \hat{\boldsymbol{x}})$, and $K(\boldsymbol{x}, \hat{\boldsymbol{x}})$ is the conductivity of the t-bond. We assume symmetry: $K(\boldsymbol{x}, \hat{\boldsymbol{x}}) = K(\hat{\boldsymbol{x}}, \boldsymbol{x})$. The t-bond conductivity needs to be determined in terms of the material conductivity κ. Note that the vectors $\hat{\boldsymbol{x}} - \boldsymbol{x}$ and $\boldsymbol{e}$ are collinear and their dot product, $(\hat{\boldsymbol{x}} - \boldsymbol{x}) \cdot \boldsymbol{e}$, is simply the signed distance between the points $\hat{\boldsymbol{x}}$ and $\boldsymbol{x}$ along the bar direction.

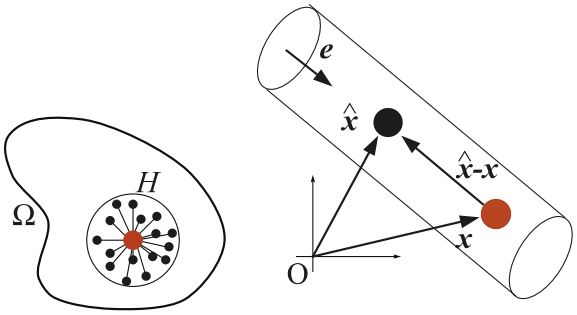

Fig. 2. The peridynamic description of a thermal body. A thermal conductor between the points $\boldsymbol{x}$ and $\hat{\boldsymbol{x}}$.

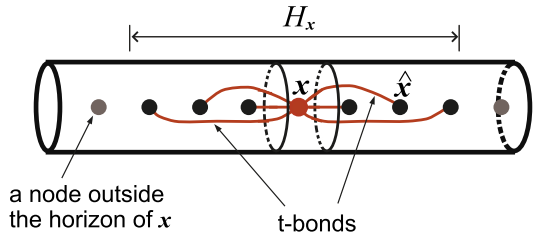

Fig. 3. The thermal bonds for one-dimensional heat transfer in a peridynamic bar. Only a small section of the bar is shown here.

Remark. Here is the point where, by taking $\hat{\boldsymbol{x}} \to \boldsymbol{x}$, we would recover the classical derivation of the heat equation. Instead, we assume the equation to hold for finite distances $\|\hat{\boldsymbol{x}} - \boldsymbol{x}\|$. Obviously, the smaller this distance, the better the approximation of the classical equation.

Dividing Eq. (5) by $(\hat{\boldsymbol{x}} - \boldsymbol{x}) \cdot \boldsymbol{e}$ and integrating over the horizon of point $\boldsymbol{x}$ we get:

$$\int_{\mathcal{H}_x} \rho c \frac{\partial \theta_a(\boldsymbol{x}, \hat{\boldsymbol{x}}, t)}{\partial t} d\hat{\boldsymbol{x}} = \int_{\mathcal{H}_x} K(\boldsymbol{x}, \hat{\boldsymbol{x}}) \frac{\theta(\hat{\boldsymbol{x}}, t) - \theta(\boldsymbol{x}, t)}{\|\hat{\boldsymbol{x}} - \boldsymbol{x}\|^2} d\hat{\boldsymbol{x}}. \tag{6}$$

We assume the following relation between the temperature at point $\boldsymbol{x}$ and time t and the average temperatures in all the t-bonds connected at $\boldsymbol{x}$:

$$\int_{\mathcal{H}_x} \rho c \theta_a(\boldsymbol{x}, \hat{\boldsymbol{x}}, t) d\hat{\boldsymbol{x}} = \rho c \theta(\boldsymbol{x}, t) V_{H_x}. \tag{7}$$

and therefore

$$\int_{\mathcal{H}_x} \rho c \frac{\partial \theta_a(\boldsymbol{x}, \hat{\boldsymbol{x}}, t)}{\partial t} d\hat{\boldsymbol{x}} = \rho c \frac{\partial \theta(\boldsymbol{x}, t)}{\partial t} V_{H_x}. \tag{8}$$

Here, V_{H_x} is the horizon volume for the node centered at $\boldsymbol{x}$. Eq. (6) now becomes:

$$\begin{aligned} \rho c \frac{\partial \theta(\boldsymbol{x}, t)}{\partial t} &= \int_{\mathcal{H}_x} k(\boldsymbol{x}, \hat{\boldsymbol{x}}) \frac{\theta(\hat{\boldsymbol{x}}, t) - \theta(\boldsymbol{x}, t)}{\|\hat{\boldsymbol{x}} - \boldsymbol{x}\|^2} d\hat{\boldsymbol{x}} \\ &= \int_{\mathcal{H}_x} \Theta(\boldsymbol{x}, \hat{\boldsymbol{x}}, \theta(\boldsymbol{x}, t), \theta(\hat{\boldsymbol{x}}, t), t) d\hat{\boldsymbol{x}}, \end{aligned} \tag{9}$$

with $k(\boldsymbol{x}, \hat{\boldsymbol{x}}) = K(\boldsymbol{x}, \hat{\boldsymbol{x}}) / V_{H_x}$ defined to be the *micro-conductivity of the t-bond* $(\boldsymbol{x}, \hat{\boldsymbol{x}})$. This is the peridynamic equation for one-dimensional heat transfer in a bar, without any heat sources. If a heat source is present at $\boldsymbol{x}$, then (9) becomes:

$$\rho c \frac{\partial \theta(\boldsymbol{x}, t)}{\partial t} = \int_{\mathcal{H}_x} k(\boldsymbol{x}, \hat{\boldsymbol{x}}) \frac{\theta(\hat{\boldsymbol{x}}, t) - \theta(\boldsymbol{x}, t)}{\|\hat{\boldsymbol{x}} - \boldsymbol{x}\|^2} d\hat{\boldsymbol{x}} + w(\boldsymbol{x}, t), \tag{10}$$

where $w(\boldsymbol{x},t)$ is the rate of heat generation per unit volume per unit time function. In contrast to the classical theory, the Eqs. (9) and (10) are applicable even when in the body cracks or other forms of damage appear and/or propagate.

Eqs. (9) and (10) represent the *conservation of energy* law, or the first law of thermodynamics, together with Fourier's law for one-dimensional heat transfer in the peridynamic formulation.

2.1. The peridynamic heat-flux

To simply the discussion, consider the following situation in one dimension, graphically described in Fig. 4: inside the horizon of a node x_i there is a monotonic change in temperature from hot (to the right) to cold (to the left). The definitions that follow are valid for any distribution of temperatures within the horizon.

In order to compute the peridynamic heat-flux (which is the rate at which heat is transferred at a point across a given surface

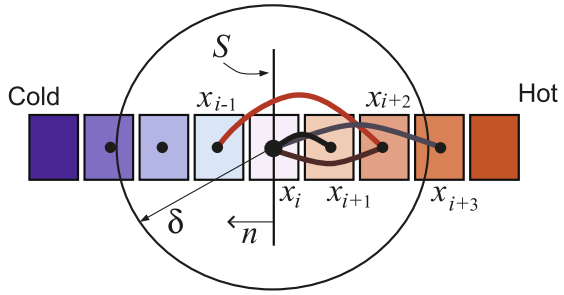

Fig. 4. The peridynamic description of the heat-flux at a point x_i across a given surface at that point. The thermal conductors ending at x_i from one side of the bar contribute to the heat-flux at x_i, but the thermal conductor between the points x_{i+2} and x_{i-1} does not. Only a portion from the heat-flux through the conductor (x_i, x_{i+3}), proportional to the volume of x_{i+3} inside the horizon of x_i, contributes to the total heat-flux at x_i.

at that point, per unit area and per unit time) at a point across a surface, we need to compute the integral of heat-fluxes through all the t-bonds that connect the point $\boldsymbol{x}$ with other points in the body and are on one side of the given surface. Note that we could, possibly, define the heat-flux through the surface at a point by including all bonds passing through that surface, as it is done in in the peridynamic formulation for elasticity for the "force fluxes" [22,40].

The heat loss/gain at $\boldsymbol{x}$ due to its connection to $\hat{\boldsymbol{x}}$ is due to the heat-flux between $\boldsymbol{x}$ and $\hat{\boldsymbol{x}}$ along the t-bond $(\boldsymbol{x}, \hat{\boldsymbol{x}})$ which is given by

$$Q(\boldsymbol{x}, \hat{\boldsymbol{x}} - \boldsymbol{x}, t) = -k(\boldsymbol{x}, \hat{\boldsymbol{x}}) \frac{\theta(\hat{\boldsymbol{x}}, t) - \theta(\boldsymbol{x}, t)}{(\hat{\boldsymbol{x}} - \boldsymbol{x}) \cdot \boldsymbol{e}}. \tag{11}$$

The equation above is the peridynamic form of Fourier's law, written for a t-bond. This heat-flux along a t-bond is an odd function of its direction, that is $Q(\boldsymbol{x}, \hat{\boldsymbol{x}} - \boldsymbol{x}, t) = -Q(\boldsymbol{x}, \boldsymbol{x} - \hat{\boldsymbol{x}}, t)$. The function $k(\boldsymbol{x}, \hat{\boldsymbol{x}})$ is the *micro-conductivity function* of the t-bond $(\boldsymbol{x}, \hat{\boldsymbol{x}})$. For a homogeneous material, the micro-conductivity function will be the same for all t-bonds in the body. For a thermally isotropic body, the micro-conductivity depends on the vector $\boldsymbol{x} - \hat{\boldsymbol{x}}$ only through its magnitude. The dependence of the micro-conductivity on the relative distance between $\boldsymbol{x}$ and $\hat{\boldsymbol{x}}$ may take various forms. Some possible options are detailed in Section 2.3. In Section 2.3 we shall also see how the micro-conductivity relates to the conductivity of the material and the horizon at point $\boldsymbol{x}$. The micro-conductivity function may also depend on the orientation of the thermal bond $(\boldsymbol{x}, \hat{\boldsymbol{x}})$. This allows a direct modeling (and an easy implementation) of thermally anisotropic materials. The micro-conductivity function may also depend on temperature, damage index etc., but these things are not considered in the present work.

To find the peridynamic heat-flux at some point $\boldsymbol{x}$ (x_i in Fig. 4) across the surface S at $\boldsymbol{x}$ we refer to Fig. 4. The t-bonds ending at $\boldsymbol{x}$ from one side of the surface S contribute to the heat-flux at $\boldsymbol{x}$, but t-bonds between points on different sides of the surface, that do not start or end at $\boldsymbol{x}$ do not (see, e.g., the t-bond between x_{i+2} and x_{i-1} in Fig. 4). Mathematically, this leads to the following definition of the peridynamic heat-flux:

$$Q(\boldsymbol{x}, S, t) = -\int_{\mathcal{H}_{\boldsymbol{x}}/S} k(\boldsymbol{x}, \hat{\boldsymbol{x}}) \frac{\theta(\hat{\boldsymbol{x}}, t) - \theta(\boldsymbol{x}, t)}{(\hat{\boldsymbol{x}} - \boldsymbol{x}) \cdot \boldsymbol{n}} d\hat{\boldsymbol{x}} \tag{12}$$

where by $\mathcal{H}_{\boldsymbol{x}}/S$ we mean the portion of $\mathcal{H}_{\boldsymbol{x}}$ on one side of the surface S, and $\boldsymbol{n}$ is the exterior normal to the surface (in this case of a 1D bar $\boldsymbol{n} = \boldsymbol{e}$ or $\boldsymbol{n} = -\boldsymbol{e}$). The definition is valid for any arbitrary distribution of temperatures around x_i.

2.2. A thermal material with damage

To introduce damage in the current formulation we proceed in a similar way in which damage is introduced in the mechanical PD formulation [26]. The function Θ in (9) is replaced by a *history-dependent* function:

$$\widetilde{\Theta}(\boldsymbol{x}, \hat{\boldsymbol{x}}, \theta(\boldsymbol{x}, t), \theta(\hat{\boldsymbol{x}}, t), t) = \Theta(\boldsymbol{x}, \hat{\boldsymbol{x}}, \theta(\boldsymbol{x}, t), \theta(\hat{\boldsymbol{x}}, t), t) \mu(t, \|\hat{\boldsymbol{x}} - \boldsymbol{x}\|) \tag{13}$$

where μ is a history-dependent scalar-value function defined by

$$\mu(t, \|\hat{\boldsymbol{x}} - \boldsymbol{x}\|) = \begin{cases} 1, & \text{if} \quad e(\tau, \xi, \eta) < e_0 \quad \text{for all} \quad 0 \leqslant \tau \leqslant t \\ 0, & \text{otherwise} \end{cases} \tag{14}$$

where

$$e = \frac{\|\xi + \eta\| - \|\xi\|}{\|\xi\|} \tag{15}$$

is the *relative elongation* of a bond, e_0 is the critical relative elongation of the bond, $\xi = \hat{\boldsymbol{x}} - \boldsymbol{x}$ is the relative position vector in the initial configuration and $\eta = \hat{\boldsymbol{u}} - \boldsymbol{u}$ is the relative displacement vector. This history-dependence leads to heat-transfer interruption between $\boldsymbol{x}$ and $\hat{\boldsymbol{x}}$ when the mechanical bond is broken. In peridynamics crack surfaces form when the peridynamic bonds break in succession. Heat transfer may still take place between the crack surfaces by convection or radiation. In addition, heat transfer by conduction may, partially or fully, resume if the crack closes and contact between the crack surfaces takes place. In such a case, the function in (14) needs to be modified accordingly. These subjects are topics of future study and will be reported in forthcoming publications.

2.3. The relation between material conductivity and micro-conductivity: the 1D case

In order to connect the peridynamic micro-conductivity function introduced in (5) and (9) to the measurable material conductivity κ we use the following approach. Consider two materials: a classical material with thermal conductivity κ, and a "micro-thermal" material characterized by the peridynamic heat-transfer equations and the micro-conductivity function k. Consider steady-state heat transfer in 1D in two bars made out of the classical and micro-thermal materials over which a linear temperature field is given as $\theta(x,t) = ax + b$, with a and b given constants (see Fig. 5). We impose that the heat-flux at point x through the surface S (see Fig. 5) be the same in both bars. Thus, in the classical material at

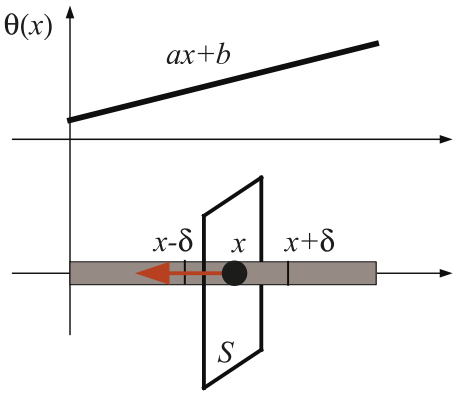

Fig. 5. Setup for the connection between the micro-conductivity and the classical conductivity. For the same given temperature $\theta(x, t) = ax + b$ the heat-flux passing though the surface S in the classical material is matched with the same quantity in the micro-thermal material. The horizon of point x is δ.

some point x along the bar through the surface S, from right to left, we have:

$$q(x,t) = \kappa \frac{\partial \theta(x,t)}{\partial x} = \kappa a.$$

In the micro-thermal material, the heat-flux through the surface S at point x, from right to left, is given by

$$q_{\text{peri}}(x,t) = \int_0^{\delta} k(|\hat{x}-x|)\frac{\theta(\hat{x})-\theta(x)}{\hat{x}-x}d\hat{x}$$

The specific form of the micro-conductivity function is expected to have an influence at scales of the order of the horizon size. In the limit of the horizon going to zero we expect to recover the solution of the classical, local heat-transfer equations, as discussed in the derivations in Section 2.

2.3.1. Constant micro-conductivity function

The simplest form of the micro-conductivity function is a constant function over the horizon (as shown in Fig. 6a):

$$k(|\hat{x}-x|) = k_0 = \text{constant}$$

Equating $q(x,t)$ and $q_{\text{peri}}(x,t)$ gives:

$$k_0 = \frac{\kappa}{\delta}, \tag{16}$$

where δ is the horizon size.

2.3.2. Triangular micro-conductivity function

A "triangular" micro-conductivity function is defined by (see Fig. 6b):

$$k(|\hat{x}-x|) = k_1\left(1-\frac{|\hat{x}-x|}{\delta}\right).$$

Equating again $q(x,t)$ and $q_{\text{peri}}(x,t)$ we obtain:

$$k_1 = \frac{2\kappa}{\delta}. \tag{17}$$

3. Numerical discretization in 1D

To implement the peridynamic method for heat conduction in 1D, we discretize the domain using a uniform grid. Non-uniform grids are possible in peridynamics (see [39]) but this is not pursued here. Each node has a "volume", in 1D given by the length of the segment associated with it, in our case Δx. Fig. 4 shows nodes within the horizon of the i-th node. The nodes at the ends have the coordinates $-L/2 + \Delta x/2$ and $L/2 - \Delta x/2$. Other options can be selected: for example, we can place nodes at the actual ends of the bar in which case these end nodes will have half-volumes (see, e.g., [39]). We have performed numerical tests using both methods and found out that there are no differences between them. The results we report below use the first method, with all nodes having the same volume (length).

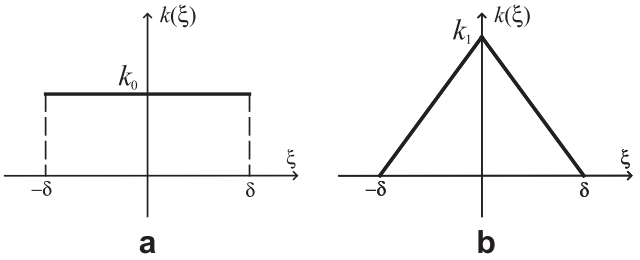

Fig. 6. Two sample functions for the micro-conductivity variation inside the peridynamic horizon.

The spatial discretization of Eq. (9), using a mid-point type numerical integration, is

$$\rho c\dot{\theta}(x_i,t) = \sum_p k(x_i,x_p)\frac{\theta(x_p,t)-\theta(x_i,t)}{(x_p-x_i)^2}V_{ip}, \tag{18}$$

where the summation is after all nodes x_p inside the horizon of node x_i, and V_{ip} is the portion of the volume of the node x_p actually covered by the horizon of node x_i. Note that special care has to be taken when computing the term for $p = i$. In the limit of $x_p \to x_i$ this term represents the spatial rate of change of the heat-flux in the t-bond (x_i, x_p). Also note that the limit $x_p \to x_i$ can take place only when their corresponding volumes go to zero, otherwise we violate the principle of interpenetration of matter. We compute the above-mentioned term by approximating it with:

$$\frac{1}{2}\left[k(x_{i-1},x_i)\frac{\theta(x_{i-1},t)-\theta(x_i,t)}{(x_{i-1}-x_i)^2}V_{i,i-1} + k(x_i,x_{i+1})\frac{\theta(x_{i+1},t)-\theta(x_i,t)}{(x_{i+1}-x_i)^2}V_{i,i+1}\right].$$

In a body that undergoes damage, if one of the mechanical bonds (x_{i-1},x_i) or (x_i,x_{i+1}) gets broken and interrupts the heat transfer then the $p = i$ term is computed to be the same as the $p = i - 1$ or the $p = i + 1$ terms. For the time integration we use a Runge–Kutta integration which is a fourth-order explicit method.

For numerically evaluating the heat-flux in Eq. (12), from right to left for example, we use mid-point integration:

$$q(x,t) = -\sum_p k(x_i,x_p)\frac{\theta(x_p,t)-\theta(x_i,t)}{x_p-x_i}V_{ip}, \tag{19}$$

where the summation is after all nodes x_p on the right side of the surface at x_i inside the horizon, δ, of node x_i. In the case $p = i$, we approximate the term in the sum by

$$k(x_i)\frac{\theta(x_{i+1},t)-\theta(x_i,t)}{x_{i+1}-x_i}(V_i/2) \tag{20}$$

which is the heat-flux from the right-half of the volume of x_i,$V_i/2$. This approximation can be easily extend to higher dimensions. For the triangular micro-conductivity case we use $k(x_i) = k_1$ instead of $k_1(1-\frac{|x_{i+1}-x_i|}{\delta})$ since the portion that conducts heat is the volume of x_i not of x_{i+1}.

3.1. Imposing Dirichlet (temperature) boundary conditions

For the discretization type mentioned above, in which all nodes have the same volume, we impose the Dirichlet boundary conditions by simply assigning the given temperature value to the end node or nodes. In effect, the entire volume of the node is assigned the given boundary temperature. In the numerical examples we will discuss the implications of this observation to the comparison with the exact classical solutions of heat transfer. In the limit of the horizon going to zero (which induces the nodal volume to go to zero; see the definition of the δ-convergence) the peridynamic Dirichlet condition converges to the classical boundary condition.

3.2. Imposing Neumann (heat-flux) boundary conditions

We discuss here the way heat-flux boundary conditions can be implemented in our new peridynamic formulation for heat transfer, for the case of constant heat-flux. The general case can be treated similarly.

In peridynamics, a given constant heat-flux q boundary condition applied at a boundary node x reads:

$$q = q_{\text{peri}}(x,t) = \int_0^{\delta} k(|\hat{x}-x|)\frac{\theta(\hat{x},t)-\theta(x,t)}{\hat{x}-x}d\hat{x}. \tag{21}$$

We approximate this boundary condition by imposing that the temperature of the nodes inside the horizon of the, for example, left end node are connected by the following relationships that need to hold at all times:

$$\theta_{m+1-i} = \theta_{m+1} + i\Delta x\frac{q}{\kappa} \quad i = 1,\ldots,m, \tag{22}$$

where κ is the thermal conductivity, Δx is the nodal volume (for a uniform discretization), and $m = \delta/\Delta x$ is related to the number of nodes inside the horizon. Similar relationships can be written for the right end node. Note that the initial condition is applied only to θ_{m+1} while the $\theta_1,\ldots,\theta_m$ values are computed based on the formulas above. The same happens at all time steps, when θ_{m+1} is computed from the general discretization, and the temperatures at the first m nodes are updated using (22). See Fig. for an example when $m = 3$.

We can show that if Eq. (22) are satisfied then Eq. (21) holds at the boundary in the limit of the horizon going to zero. The short proofs for the constant and triangular micro-conductivities are given below.

Indeed, for the case of constant micro-conductivity, from Eqs. (21) and (22) we get, at a specific time:

$$q_{peri}(x_1) = \int_0^{\delta} k(\hat{x})\frac{\theta(\hat{x})-\theta(x)}{\hat{x}-x}d\hat{x} \approx k_0\sum_{i=1}^{m+1}\frac{\theta_i-\theta_1}{x_i-x_1}V_{1i} \tag{23}$$

$$\approx \Delta x k_0\left[\frac{\theta_2-\theta_1}{2\Delta x}+\frac{\theta_2-\theta_1}{\Delta x}+\cdots + \frac{\theta_m-\theta_1}{(m-1)\Delta x}+\frac{\theta_{m+1}-\theta_1}{2m\Delta x}\right] \tag{24}$$

$$= \Delta x k_0\left[\underbrace{\frac{q}{\kappa}+\frac{q}{\kappa}+\cdots+\frac{q}{\kappa}}_{m}\right] = \Delta x\frac{\kappa}{\delta}m\frac{q}{\kappa} = q. \tag{25}$$

The approximation signs become equalities in the limit of the horizon going to zero.

For the triangular micro-conductivity case we have:

$$q_{peri}(x_1) = \int_0^{\delta} k(\hat{x})\frac{\theta(\hat{x})-\theta(x)}{\hat{x}-x}d\hat{x}$$

$$\approx k_1\sum_{i=1}^{m+1}\left(1-\frac{|x_i-x_1|}{\delta}\right)\frac{\theta_i-\theta_1}{x_i-x_1}V_{1i} \tag{26}$$

$$\approx \Delta x k_1\left[\frac{\theta_2-\theta_1}{2\Delta x}+\left(1-\frac{\Delta x}{m\Delta x}\right)\frac{\theta_2-\theta_1}{\Delta x}+\cdots + \left(1-\frac{m\Delta x}{m\Delta x}\right)\frac{\theta_{m+1}-\theta_1}{2m\Delta x}\right]$$

$$= \Delta x k_1\left[\frac{q}{2\kappa}+\left(1-\frac{1}{m}\right)\frac{q}{\kappa}+\cdots+\left(1-\frac{m-1}{m}\right)\frac{q}{\kappa}\right]$$

$$= \frac{q}{\kappa}\Delta x k_1\frac{m}{2} = q. \tag{27}$$

As above, approximation signs become equalities in the limit of the horizon going to zero.

4. Comparison with classical heat conduction for transient problems in 1D

Here we test the convergence to the solution of the classical transient heat-conduction equations for two examples: one with Dirichlet boundary conditions (temperature values given) at both ends of the bar and one with a Neumann condition (heat-flux given) at one end and Dirichlet condition at the other end. The analytical solutions are obtained using separation of variables (see [41, pp. 954–963]). To numerically compute the infinite series solutions we used certain number of terms and the details are given below. The coefficient α in the second problem is different than in [41] in order to speed-up the heat transfer.

4.1. Classical formulations of the problems

4.1.1. Example 1

A rod of length $L = 10$ cm has an initial temperature 100 °C. The left and right sides of this rod are suddenly brought to and maintained at a temperature of 0 °C. The thermal diffusivity is $\alpha = 1.14\ \text{cm}^2/\text{s}$. We are interested in the changes of the temperature profile in time. The classical formulation for this problem is as follows:

$$\frac{\partial\theta(x,t)}{\partial t} = \alpha\frac{\partial^2\theta(x,t)}{\partial x^2}, \quad 0 < x < L, \quad 0 \leqslant t < \infty, \tag{28}$$

$$\theta(0,t) = \theta(L,t) = 0, \quad 0 \leqslant t < \infty, \tag{29}$$

$$\theta(x,0) = 100, \quad 0 < x < L, \tag{30}$$

Using the method of separation of variables and the numerical values given above, the exact solution can be written in a series form as

$$\theta(x,t) = \theta(0,t) + (\theta(L,t)-\theta(0,t))\frac{x}{L} + \sum_{n=1,3,5,\ldots}^{\infty} K_n\sin\frac{n\pi x}{L}e^{-\alpha t(n^2\pi^2/L^2)}, \tag{31}$$

where

$$K_n = \frac{2}{L}\int_0^L \theta(x,0)\sin\frac{n\pi x}{L}dx. \tag{32}$$

Then,

$$\theta(x,t) = \theta(0,t) + (\theta(L,t)-\theta(0,t))\frac{x}{L} + \frac{4}{\pi}\theta(x,0) \times \sum_{n=1,3,5,\ldots}^{\infty}\sin\frac{n\pi x}{L}e^{-\alpha t(n^2\pi^2/L^2)}, \tag{33}$$

Also, the exact classical heat-flux is

$$q(x,t) = \frac{4\kappa}{10}\theta(x,0)\sum_{n=1,3,5,\ldots}^{\infty}\cos\frac{n\pi x}{L}e^{-\alpha t(n^2\pi^2/L^2)}. \tag{34}$$

4.1.2. Example 2

The left end of a rod of length $L = 10$ cm is insulated, and the right end is held at a constant temperature 100 °C for all $t \geqslant 0$. The initial temperature is 60 °C for $0 < x < L/2$ and 0 °C for $L/2 < x < L$. The same diffusivity as above is used: $\alpha = 1.14\ \text{cm}^2/\text{s}$. The classical formulation is

$$\frac{\partial\theta(x,t)}{\partial t} = \alpha\frac{\partial^2\theta(x,t)}{\partial x^2}, \quad 0 < x < L, \quad 0 \leqslant t < \infty, \tag{35}$$

$$\frac{\partial\theta(0,t)}{\partial x} = 0, \quad \theta(L,t) = 100, \quad 0 \leqslant t < \infty \tag{36}$$

$$\theta(x,0) = \begin{cases} 60, & 0 < x < L/2; \\ 0, & L/2 < x < L. \end{cases} \tag{37}$$

The exact solution in this case is

$$\theta(x,t) = \theta(L,t) + \frac{4}{\pi}\sum_{n=1,3,5,\ldots}^{\infty}\frac{1}{n}\left[(\theta_1(x,0)-\theta(L,t))\sin\frac{n\pi}{4} - (\theta_2(x,0) - \theta(L,t))\left(\sin\frac{n\pi}{2}-\sin\frac{n\pi}{4}\right)\right]\cos\frac{n\pi x}{2L}e^{-\alpha t(n^2\pi^2/4L^2)}, \tag{38}$$

where $\theta_1(x,0)$ and $\theta_2(x,0)$ are the left and right parts of $\theta(x,0)$. Similarly, the exact classical heat-flux is

$$q(x,t) = -\frac{2}{L}\sum_{n=1,3,5,\ldots}^{\infty}\Big[(\theta_1(x,0)-\theta(L,t))\sin\frac{n\pi}{4} - (\theta_2(x,0) - \theta(L,t))\Big(\sin\frac{n\pi}{2} - \sin\frac{n\pi}{4}\Big)\Big]\sin\frac{n\pi x}{2L}e^{-\alpha t(n^2\pi^2/4L^2)}. \quad (39)$$

4.1.3. Example 3

We also test our implementation for a problem in which a non-zero heat-flux is imposed on one boundary.

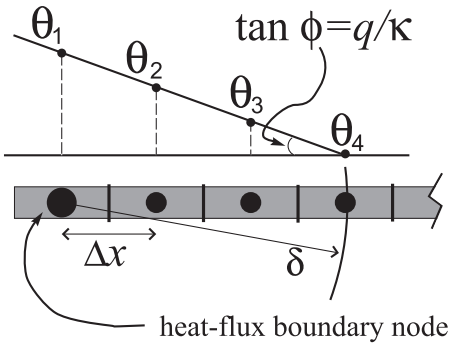

Fig. 7. Imposing heat-flux boundary condition at left-end of the bar for the case when the heat-flux is constant. The relation between the nodal temperatures of the nodes within the horizon of the boundary node, the imposed heat-flux value, q, and the thermal conductivity, κ, when $m = 3$.

A rod of length $L = \pi$ cm has an initial temperature 0 °C. The left end of this rod is maintained at a temperature of 20 °C while at the right end a heat-flux 3κ W/cm^2 is imposed (κ is the thermal conductivity). The thermal diffusivity is $\alpha = 1.14$ cm^2/s. The classical formulation for this problem is as follows:

$$\frac{\partial\theta(x,t)}{\partial t} = \alpha\frac{\partial^2\theta(x,t)}{\partial x^2}, \quad 0 < x < \pi, \quad 0 \leqslant t < \infty, \quad (40)$$

$$\theta(0,t) = 20, \quad \theta_x(L,t) = 3, \quad 0 \leqslant t < \infty, \quad (41)$$

$$\theta(x,0) = 0, \quad 0 < x < \pi. \quad (42)$$

Using the method of separation of variables and the numerical values given above, the exact solution can be written in a series form as

$$\theta(x,t) = 20 + 3x + \sum_{n=1,3,5,\ldots}^{\infty} K_n \sin\frac{nx}{2}e^{-\alpha t(n^2/4)}, \quad (43)$$

where

$$K_n = \frac{2}{L}\left(\frac{40+6L}{n}\cos\frac{nL}{2} - \frac{12}{n^2}\sin\frac{nL}{2} - \frac{40}{n}\right). \quad (44)$$

Remark. The peridynamic formulations for these examples are given by Eq. (9) with the micro-conductivity given by, for example, Eq. (16) or Eq. (17), and the corresponding associated boundary conditions. Note that the Dirichlet and Neumann boundary

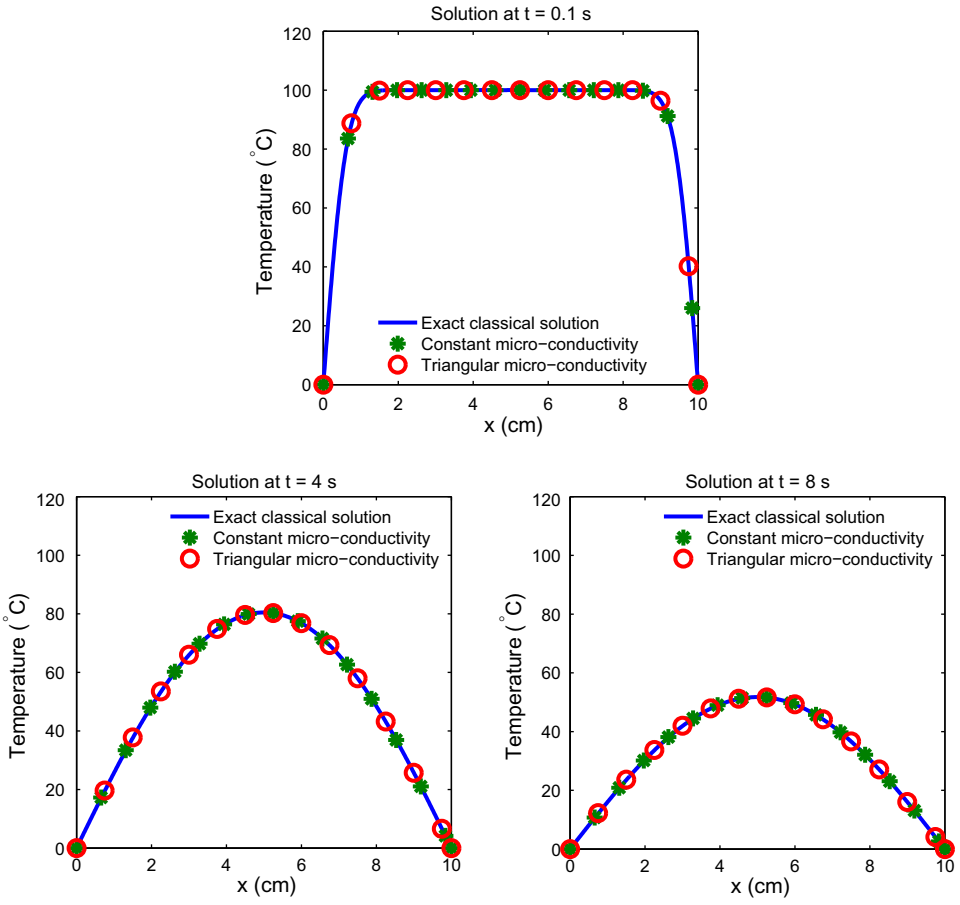

Fig. 8. Example 1: comparison between the classical exact solution and the peridynamic solutions for the constant and triangular micro-conductivities. The particular values used here are $\delta = 4\Delta x$ and $\Delta x = L/800$.

conditions are imposed as described in Sections 3.1 and 3.2, respectively. Due to the constructive formulation, the peridynamic equation converges to the classical PDE, while the peridynamic boundary conditions converge, in the limit of the horizon going to zero, to the classical boundary conditions, as detailed in Sections 3.1 and 3.2.

4.2. Numerical results

We use the fourth-order time integration Runge–Kutta method. We select a time step $\Delta t = 10^{-6}$ in all tests as this is a stable time step for the smallest grid size we used in this section.

4.2.1. Results for Examples 1 and 2

The exact classical solution and the peridynamic solutions using the constant and the triangular micro-modulus for the case when $\delta = 3L/800 = 0.0375$ cm, the number of nodes is 1067 (and therefore $m = \delta/\Delta x = 4$) are plotted in Figs. 7 and 8 for Example 1 and in Fig. 9 for Example 2. For better clarity, we plot the analytical solution at all nodes, and the peridynamic solution with the constant micro-modulus at 15 equally-spaced nodes and with the triangular micro-conductivity at 14 nodes. To compute the analytical solution, for Example 1 we truncated the series after $n = 55$ for $t = 0.1$ s, $n = 9$ for $t = 4$ s, and $n = 5$ for $t = 8$ s. For the second Example we truncated after $n = 109$ for $t = 0.1$ s, $n = 17$ for $t = 4$ s, and $n = 13$ for $t = 8$ s.

We also compare, in norm-2, the difference between the peridynamic solution and the local (or classical) analytical solution. We do not call this difference an "error" because we are not comparing with the analytical solution of the nonlocal problem (defined by Eq. (10)). The nonlocal exact solution is not available, as solutions to integro-differential equations are, in general, more difficult to obtain than solutions to PDE's. For the square of norm-2 we use the average relative difference defined as

$$\frac{1}{N}\sum_{i=1}^{N}\left(\frac{\theta_{\text{classical}} - \theta_{\text{peri}}}{\theta_{\text{classical}}}\right)^2, \tag{45}$$

where N is the number of all nodes used in every numerical test.

We focus the analysis on two types of convergence defined in [39]: the m-convergence, and the δ convergence. We recall (see [39]) that in the m-convergence we consider the horizon δ fixed and take $m \to \infty$. The numerical peridynamic approximation will converge to the exact nonlocal peridynamic solution for the given δ. In the case of δ-convergence, the horizon $\delta \to$ while m is fixed or increases with decreasing δ, but at a slower rate than that of δ. For problems with no singularities (which is the case of the present study), the numerical peridynamic approximation converges to the classical local solution. For problems with singularities the (δm)-convergence is needed to ensure uniform convergence (with the possible exception of points in sets of measure zero) to the local solution (see [39]).

m-convergence. For several different horizons, namely $\delta = 3L/100$, $3L/200$, $3L/400$, $3L/800$, we perform the m-convergence tests. In Fig. 10 we plot the temperatures of the peridynamic solutions at the middle node of the bar at $t = 8$ s (the end of the simulation), for values of m equal to 2, 4, 8, and 16, for both examples and both the constant and triangular micro-conductivities. We also draw the level of temperature at the same location and time, for comparison purposes only, since the numerical peridynamic

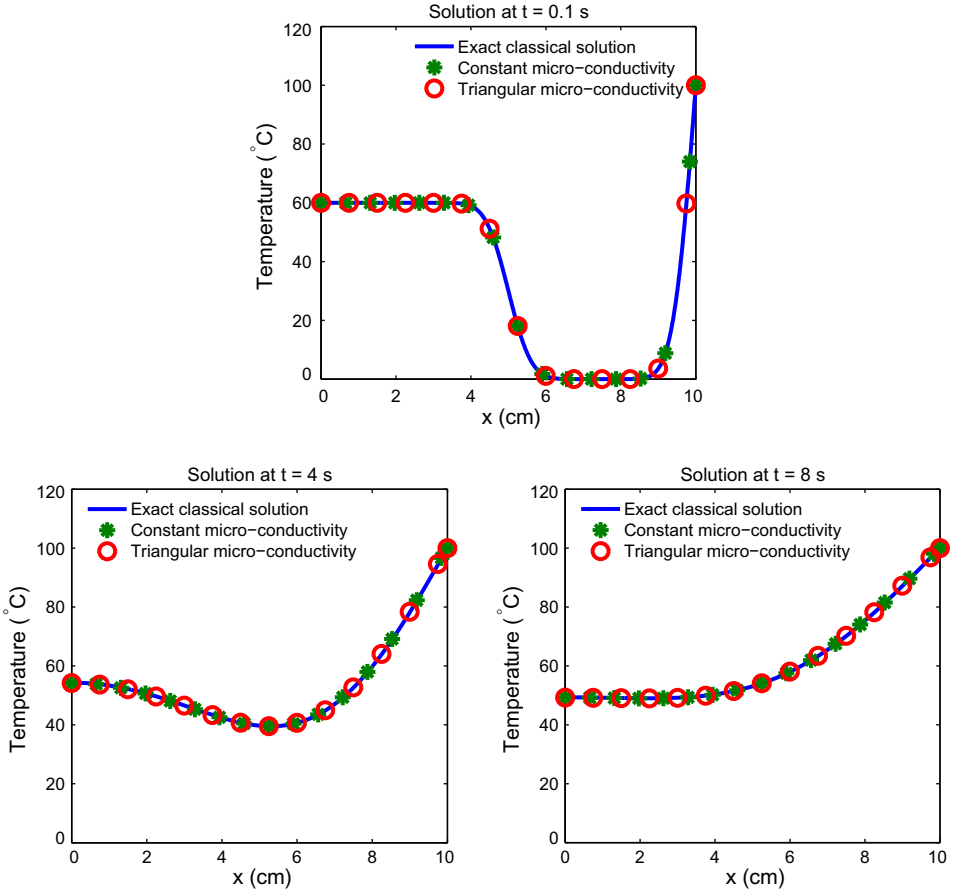

Fig. 9. Example 2: comparison between the classical exact solution and the peridynamic solutions for the constant and triangular micro-conductivities. The particular values used here are $\delta = 4\Delta x$ and $\Delta x = L/800$.

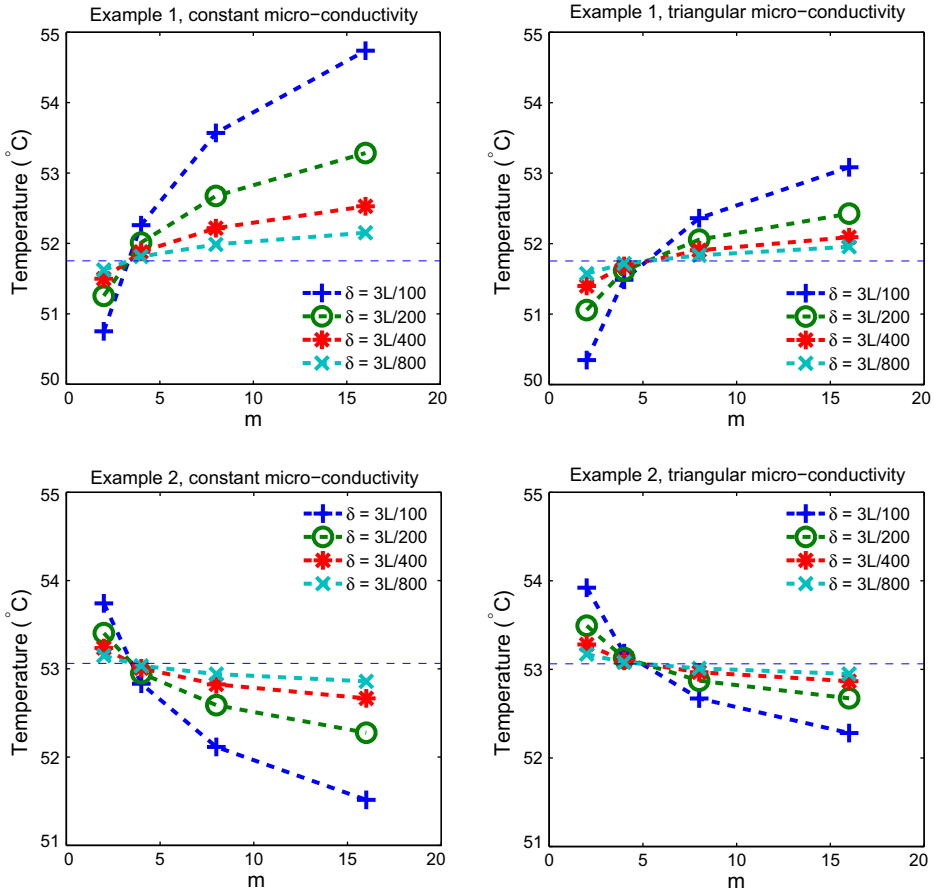

Fig. 10. The m-convergence for four different horizon sizes. Top row for Example 1 (constant micro-conductivity is left), bottom row for Example 2 (triangular micro-conductivity is right). The temperature at the middle of the bar at $t = 8$ s is plotted for different values of m and different horizon sizes. The dashed lines indicate, for comparison only, the classical exact temperature, which is 51.75 °C for Example 1 and 53.06 °C for Example 2.

solution will converge to the exact nonlocal solution. Of course, the smaller the horizon size, the closer the nonlocal solution will be to the local solution, as it can be seen by looking at the values for a fixed m but decreasing values of the horizon δ. We observe that, for every horizon size, changes in the solution slow down as m increases, which shows that we approach the exact nonlocal solution.

We now explain the behavior see in Fig. 10 for the m-convergence tests. For a fixed horizon, when m increases, the number of nodes increases and the volume (length) of each node decreases. Therefore, the peridynamic boundary condition imposes the fixed temperature over a smaller volume (length) as m increases. If the imposed temperatures at the boundaries where smaller than the initial temperature, one expects that the mid-point temperature to rise with increasing values of m, and indeed this is what we see happens in Example 1. We also observe that the triangular micro-conductivity leads to a faster m convergence. Note also that for $m = 2$, the triangular micro-conductivity results are "worse" (relative to the classical solution) than the constant micro-conductivity and that is because in the discretization for the triangular micro-conductivity we "loose" a significant chunk of the material since the micro-conductivity at the last node inside the horizon is zero (see Fig. 6 and Eq. (18)).

For Example 2, we notice a similar m-convergence behavior (see the second row of plots in Fig. 10). We also notice that, since the boundary temperature at the right end is maintained higher than the initial temperatures along the bar, we expect, following the same argument as above, that when m increases (the volume of the node with the imposed temperature decreases, the mid-point temperature, at a certain time, to be lower the higher m is). Indeed, this is what is obtained in the numerical results, for both micro-conductivity functions. The triangular micro-conductivity, again, has faster m-convergence compared to the constant micro-conductivity. For $m = 2$, the same argument as above can be repeated to explain why the values from the triangular case are "worse" than those for the constant case.

Remark. We also note that the m-convergence curves in the results of Fig. 10 indicate a good candidate for the number of nodes inside the horizon to use in practice if we try to obtain solutions close to the classical ones. This is given by the values of m for which the m-convergence curves for different horizons intersect. It is interesting to note that these curves appear to all pass through the same point (for each of the examples tested and for either micro-modulus function used) and the temperature for that value of m is also the exact classical temperature.

If this observation holds true in general, we could compute the classical solution at a point and at an instant of time not by taking the horizon to go to zero, but by using two m-convergence curves for two different horizons of finite sizes and noting whether these curves intersect. The intersection point would be the exact classical solution. This topic is subject of further research.

From Fig. 10 we see that values of m between 3 and 5 are ideal, with the smaller values better for the constant micro-conductivity and the larger ones better for the triangular micro-conductivity case. In 1D this means that the horizon covers between 7 and 11 nodes.

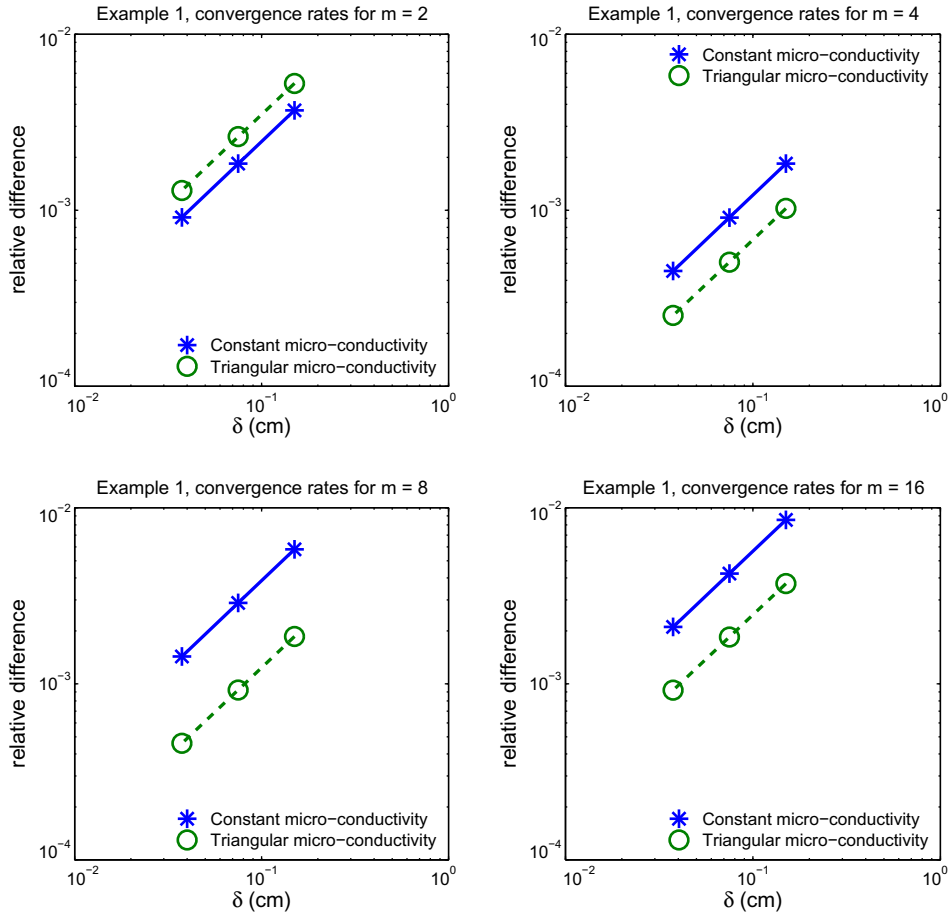

Fig. 11. The δ-convergence for the average relative difference between the classical exact solution and the peridynamic numerical solution. The difference is computed at $t = 8$ s, using (45), and for fixed values of $m = 2$, 4, 8, and 16 for Example 1. The convergence rates are linear for both micro-conductivity functions.

δ-convergence. We perform δ-convergence tests using $\delta = 3L/200$, $3L/400$, and $3L/800$ for different choices of $m = 2$, 4, 8, and 16. In Figs. 11 and 12 we plot the convergence rates, for Examples 1 and 2 respectively, for the relative difference of the temperatures along the bar at $t = 8$ s computed using the formula in (45). In Example 1, the convergence rates, obtained using linear curve fitting, for the parameters mentioned above are 1.0104, 1.0132, 1.0109, and 1.0104 respectively, for the constant micro-conductivity case and 1.0095, 1.0102, 1.0082, and 1.0055 for the triangular micro-conductivity case. In Example 2, the convergence rate are 1.4824, 1.4982, 1.4914, and 1.4811 for the constant micro-conductivity case and 1.4843, 1.4990, 1.4877, and 1.4433 for the triangular micro-conductivity case.

Note that the triangular micro-conductivity has better (smaller) relative differences compared to the exact classical solution once m is larger than 2. The reason for this is because the triangular micro-conductivity function is closer to a "localized" (Dirac-delta function) than the constant micro-conductivity function. The switched behavior for $m = 2$ can be understood based on the comments provided in the m-convergence section.

We next compute the heat-flux and compare the classical exact and the peridynamics results in Fig. 13 for Example 1 and in Fig. 14 for Example 2.

The number of nodes where we plot the heat-flux in Figs. 13 and 14 is the same and is obtained by using the values at every 40 nodes for Example 1, and every 19 nodes for Example 2.

4.2.2. Results for Example 3

This is the case for non-zero heat-flux condition at one end. Here we only perform the computations for finding the temperature field, using the both constant and triangular micro-conductivities, for a single horizon ($\delta = 3L/800 = 0.0118$ cm) and a single m value ($m = 4$). In this case the total number of nodes is 1067. The average relative difference, see Eq. (45) for this case is 3.43×10^{-5} for the constant micro-conductivity and 2.84×10^{-5} for the triangular micro-conductivity. The temperature profiles at 0.1 s, 4 s, and 8 s are shown in Fig. 15.

5. Conclusions and future work

In this paper we constructed a nonlocal formulation for transient heat (and mass) transfer problems that can be applied to problems where discontinuities appear in the material, such as in materials undergoing damage, fragmentation, or in granular systems in motion. This "peridynamic" heat-transfer formulation leads to an integro-differential equation which is obtained here following a constructive way in a similar fashion to how the classical equations of heat (and mass) transfer are introduced in the classical text by Carslaw and Jaeger. Damage is introduced at the level of the peridynamic thermal bonds. We also introduced a peridynamic heat-flux and we explained the differences compared to the similar concept given in the peridynamic literature for elasticity. We correlated the parameters in the peridynamics formulation (the micro-conductivity and the horizon) with the material conductivity for the case of constant heat-flux.

We have thoroughly analyzed numerical convergence to the classical exact solution for several problems in 1D in the limit of the peridynamic horizon going to zero. The results for two different examples, one with Dirichlet boundary conditions and one with a Neumann and a Dirichlet boundary conditions, have shown that

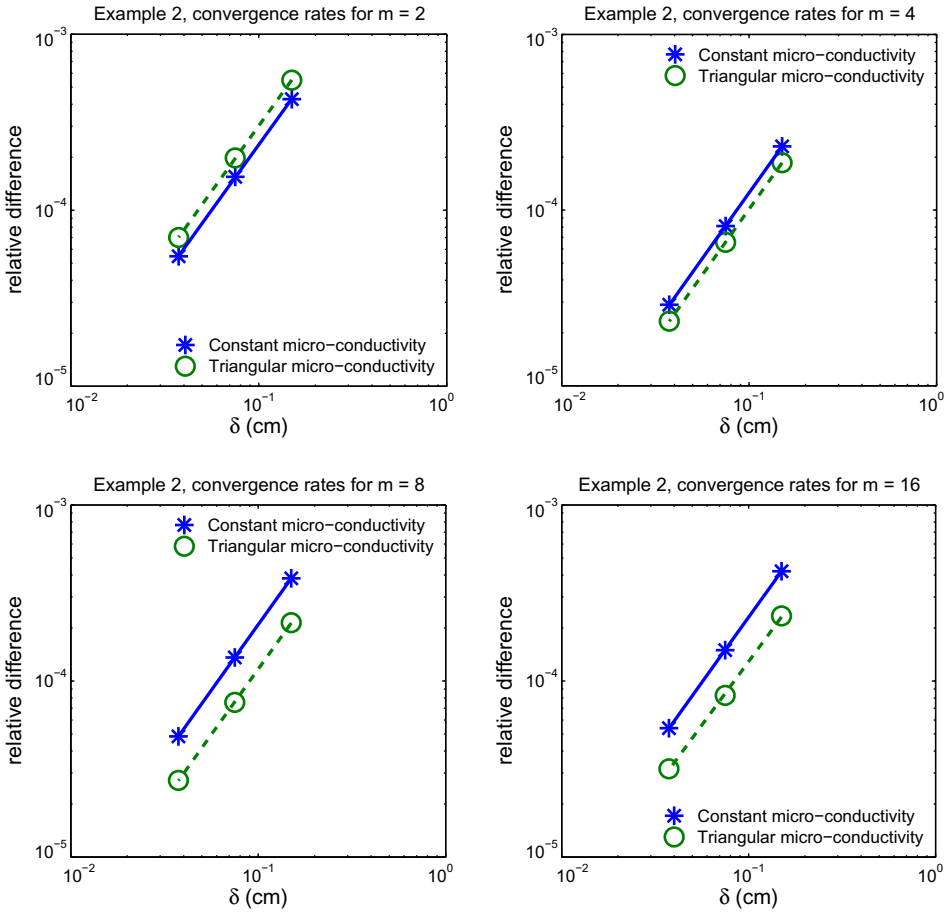

Fig. 12. The δ-convergence for the average relative difference (45) in the temperatures at $t = 8$ s and for fixed values of $m = 2, 4, 8$, and 16 for Example 2. The relative difference is between the exact classical solution and the approximate peridynamic solution. Convergence rates are super-linear (around 1.5) for both micro-conductivity functions.

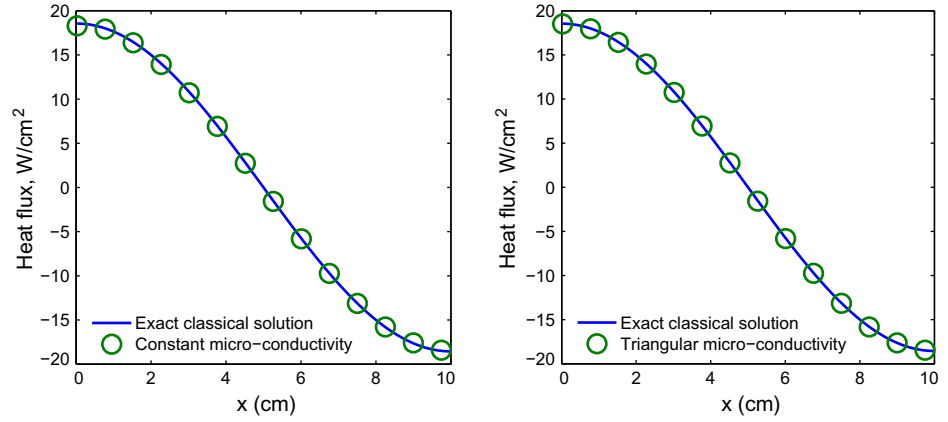

Fig. 13. Example 1: comparison of the heat-flux along the bar at $t = 8$ s for the classical exact and the peridynamics solutions. Here $\delta = 3L/800 = 0.0375$ cm and $m = 2$. Constant (left) and triangular (right) micro-conductivity.

m-convergence and δ-convergence to the classical solutions take place. For the δ-convergence we obtained linear and super-linear rates of convergence. We also noticed that a value of m between 3 and 5 (or having 7–11 nodes inside the horizon) in 1D is optimal for computations. We have tested two possible choices for the micro-conductivity function. The triangular micro-conductivity leads to results that are closer to the classical exact solution, compared to the constant micro-conductivity case, if m is larger than 2. We explained in detail how classical boundary conditions translate to the peridynamic versions. A special attention was paid to the heat-flux boundary conditions where we proved that, in the limit of the horizon going to zero, the peridynamic condition converges to the classical heat-flux boundary condition.

We also observed that if two m-convergence curves for two different horizons for the solution at a certain point and time intersect then all m-convergence curves intersect at that point, which is also the value of the classical exact solution. If this property holds true, this may provide an effective way of computing the classical exact solution not by taking the horizon to go to zero, but by finding where two m-convergence curves corresponding to two different horizons, intersect.

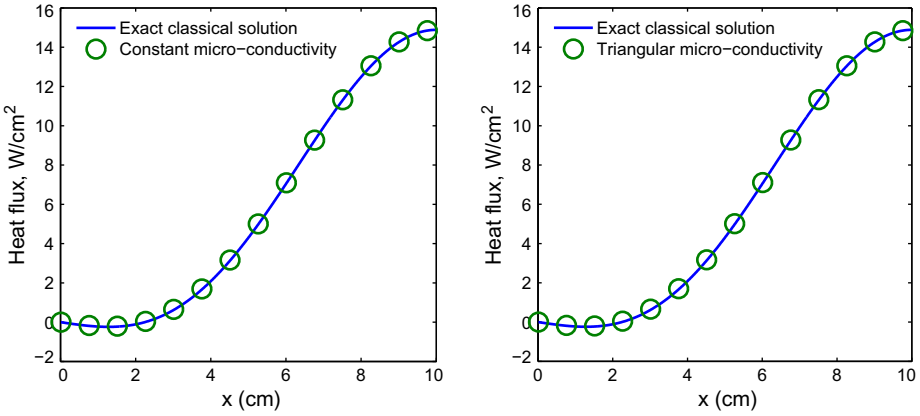

Fig. 14. Example 2: comparison of the heat-flux along the bar at $t = 8$ s for the classical exact and the peridynamics solutions. Here $\delta = 3L/800 = 0.0375$ cm and $m = 4$. Constant (left) and triangular (right) micro-conductivity.

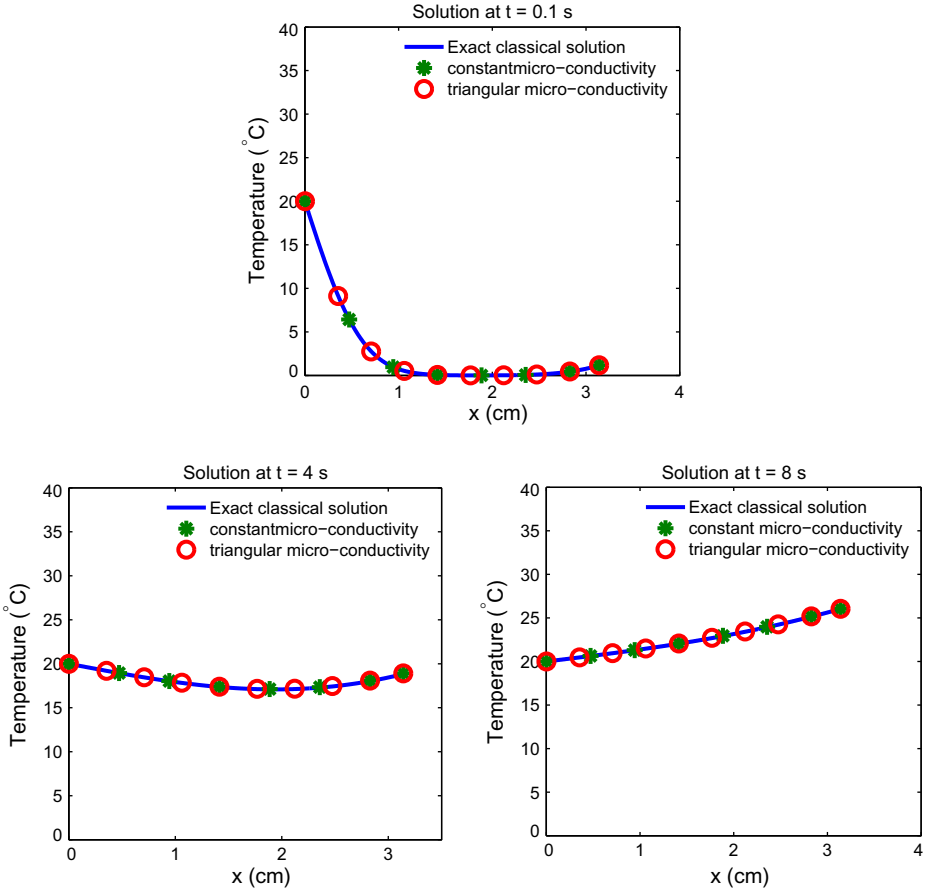

Fig. 15. The comparison between the classical exact and peridynamics solutions for Example 3. The particular values used here are $\delta = 3L/800 = 0.0118$ cm, $m = 4$.

The present formulation can be easily used for modeling heat transfer in highly heterogeneous systems and we will report such results in the future. Plans for extending the formulation to model thermomechanical fracture phenomena are currently under way.

Acknowledgements

This work has been supported, in part, by the Sandia National Laboratories, Albuquerque, NM. We are indebted to Dr. S.A. Silling for creating peridynamics. Special thanks are extended to Dr. S.A. Silling, Dr. J. Aidun, Dr. R.B. Lehoucq, and Dr. M.L. Parks for stimulating discussions that took place during a sabbatical stay in the Spring of 2009 of the first author at Sandia. The financial support and the group's extraordinary atmosphere for the sabbatical stay are gratefully acknowledged.

References

[1] J.F. Luciani, P. Mora, J. Virmont, Nonlocal heat transport due to steep temperature gradients, Phys. Rev. Lett. 51 (18) (1983) 1664–1667.
[2] G.D. Mahan, F. Claro, Nonlocal theory of thermal conductivity, Phys. Rev. B 38 (3) (1988) 1963–1969.
[3] S.L. Sobolev, Equations of transfer in non-local media, Int. J. Heat Mass Transfer 37 (14) (1994) 2175–2182.
[4] M. Grmela, G. Lebon, Finite-speed propagation of heat: a nonlocal and nonlinear approach, Physica A 248 (1998) 428–441.

[5] P. Furmanski, Effective macroscopic description for heat conduction in heteroneous materials, Int. J. Heat Mass Transfer 35 (11) (1992) 3047–3058.
[6] P. Furmanski, A mixture theory for heat conduction in heterogeneous media, Int. J. Heat Mass Transfer 37 (18) (1994) 2993–3002.
[7] A.C. Eringen, D.G.B. Edelen, On nonlocal elasticity, Int. J. Eng. Sci. 10 (3) (1972) 233–248.
[8] I.A. Kunin, Elastic Media with Microstructure I: One-Dimensional Models, first ed., Springer Press, 1982.
[9] C. A Eringen, Theory of nonlocal thermoelasticity, Int. J. Eng. Sci. 12 (12) (1974) 1063–1077.
[10] C.A. Eringen, Nonlocal theory of wave propagation in thermoelastic plates, Int. J. Eng. Sci. 29 (7) (1991) 831–843.
[11] D.G.B. Edelen, Irreversible thermodynamics of nonlocal systems, Int. J. Eng. Sci. 12 (1974) 607–631.
[12] I. Shnaid, Thermodynamically consistent description of heat conduction with finite speed of heat propagation, Int. J. Heat Mass Transfer 46 (2003) 3853–3863.
[13] B.N. Cox, H. Gao, D. Gross, D. Rittel, Modern topics and challenges in dynamic fracture, J. Mech. Phys. Solids 53 (2005) 565–596.
[14] D. Rittel, Experimental investigation of transient thermoelastic effects in dynamic fracture, Int. J. Solids Struct. 35 (22) (1998) 2959–2973.
[15] L. Jacobsson, C. Persson, S. Melin, In-situ esem study of thermo-mechanical fatigue crack propagation, Mater. Sci. Eng. A 496 (1–2) (2008) 200–208.
[16] Z.P. Bazant, M. Jirasek, Nonlocal integral formulations of plasticity and damage: survey of progress, J. Eng. Mech. 128 (11) (2002) 1119–1149.
[17] N.A. Fleck, J.W. Hutchinson, Phenomenological theory for strain gradient effects in plasticity, J. Mech. Phys. Solids 41 (12) (1993) 1825–1857.
[18] Y. Guo, Y. Huang, H. Gao, Z. Zhuang, K.C. Hwang, Taylor-based nonlocal theory of plasticity: numerical studies of the micro-indentation experiments and crack tip fields, Int. J. Solids Struct. 38 (42-43) (2001) 7447–7460.
[19] R.K. Abu Al-Rub, G.Z. Voyiadjis, Analytical and experimental determination of the material intrinsic length scale of strain gradient plasticity theory from micro- and nano-indentation experiments, Int. J. Plasticity 20 (2004) 1139–1182.
[20] G.Z. Voyiadjis, R.K. Abu Al-Rub, Gradient plasticity theory with a variable length scale parameter, Int. J. Solids Struct. 42 (2005) 3998–4029.
[21] A.G. Evans, J.W. Hutchinson, A critical assessment of theories of strain gradient plasticity, Acta Mater. 57 (5) (2009) 1675–1688.
[22] S.A. Silling, Reformulation of elasticity theory for discontinuities and long-range forces, J. Mech. Phys. Solids 48 (2000) 175–209.
[23] S.A. Silling, M. Epton, O. Weckner, J. Xu, E. Askari, Peridynamic states and constitutive modeling, J. Elasticity 88 (2007) 151–184.
[24] F.M. White, Heat and Mass Transfer, Addison Wesley, 1988.
[25] S.A. Silling, Dynamic fracture modeling with a meshfree peridynamic code, in: K.J. Bathe (Ed.), Computational Fluid and Solid Mechanics 2003, Elsevier Science Ltd, Oxford, 2003, pp. 641–644.
[26] S.A. Silling, E. Askari, A meshfree method based on the peridynamic model of solid mechanics, Comput. Struct. 83 (17-18) (2005) 1526–1535.
[27] R.W. Macek, S.A. Silling, Peridynamics via finite element analysis, Finite Elem. Anal. Des. 43 (15) (2007) 1169–1178.
[28] M.L. Parks, R.B. Lehoucq, S.J. Plimpton, S.A. Silling, Implementing peridynamics within a molecular dynamics code, Comput. Phys. Commun. 179 (11) (2008) 777–783.
[29] S.A. Silling, F. Bobaru, Peridynamic modeling of membranes and fibers, Int. J. Nonlinear Mech. 40 (2005) 395–409.
[30] F. Bobaru, Influence of van der waals forces on increasing the strength and toughness in dynamic fracture of nanofiber networks: a peridynamic approach, Model. Simul. Mater. Sci. Eng. 15 (2007) 397–417.
[31] W. Xie, Peridynamic Flux-Corrected Transport Algorithm for Shock Wave Studies. Master's Thesis, University of Nebraska-Lincoln, Department of Engineering Mechanics, Lincoln, Nebraska, 2005.
[32] J. Xu, E. Askari, O. Weckner, S.A. Silling, Peridynamic analysis of impact damage in composite laminates, J. Aerospace Eng. 21 (3) (2008) 187–194.
[33] E. Askari, F. Bobaru, R.B. Lehoucq, M.L. Parks, S.A. Silling, O. Weckner, Peridynamics for multiscale materials modeling, J. Phys. Conf. Ser. 125 (2008) 012078. 11pp.
[34] K. Dayal, K. Bhattacharya, Kinetics of phase transformations in the peridynamic formulation of continuum mechanics, J. Mech. Phys. Solids 54 (4) (2006) 1811–1842.
[35] T.L. Warren, S.A. Silling, E. Askari, O. Weckner, M.A. Epton, J. Xu, A non-ordinary state-based peridynamic method to model solid material deformation and fracture, Int. J. Solids Struct. 46 (5) (2009) 1186–1195.
[36] J.T. Foster, S.A. Silling, W.W. Chen, Viscoplasticity Using Peridynamics, Sandia Report SAND2008-7835, Sandia National Laboratories, Albuquerque, New Mexico, USA, 2008.
[37] H.S. Carslaw, J. C Jaeger, Conduction of Heat in Solids, second ed., Oxford University Press, 1959.
[38] S.A. Silling, R.B. Lehoucq, Convergence of peridynamics to classical elasticity theory, J. Elasticity 93 (2008) 13–37.
[39] F. Bobaru, M. Yang, L.F. Alves, S.A. Silling, E. Askari, J. Xu, Convergence, adaptive refinement, and scaling in 1d peridynamics, Int. J. Numer. Meth. Eng. 77 (6) (2009) 852–877.
[40] R.B. Lehoucq, S.A. Silling, Force flux and the peridynamic stress tensor, J. Mech. Phys. Solids 56 (4) (2008) 1566–1577.
[41] M.D. Greenberg, Advanced Engineering Mathematics, second ed., Pearson Education, 2005.